Chinese Chemical Letters 37 (2026) 110985

Contents lists available at ScienceDirect

Chinese Chemical Letters

journal homepage: www.elsevier.com/locate/cclet

Three birds with one stone: A multifunctional water-soluble binder for enhanced the performance of lithium-sulfur batteries

Wenyang Lei[a], Zhenwei Li[a], Hao He[a], Lan Yang[a], Xuebu Hu[a,*], Wei Liao[b], Xiaowen Yu[b], Zhongli Hu[a]

[a] College of Chemistry and Chemical Engineering, Chongqing University of Technology, Chongqing 400054, China
[b] Chongqing CEPREI Industrial Technology Research Institute Co., Ltd., Chongqing 401332, China

ARTICLE INFO

Article history:
Received 19 November 2024
Revised 13 February 2025
Accepted 20 February 2025
Available online 20 February 2025

Keywords:
Cel-SO_3Li
Binder
Nucleophilic substitution
LIPSs
Li-S batteries

ABSTRACT

Though polyvinylidene fluoride (PVDF) is commonly employed as a binder for lithium-sulfur (Li-S) batteries, it still faces the challenge of serious electrode fracture caused by dramatic volume changes during cycling, and lacks extended functions such as capturing dissolved lithium polysulfides (LIPSs) and promoting Li^+ transfer. Herein, a multifunctional water-soluble binder lithium sulfonated cellulose (Cel-SO_3Li) is designed and prepared. The Cel-SO_3Li binder can capture LIPSs due to nucleophilic substitution reaction between -SO_4Li and dissolved LIPSs. Its abundant hydroxyl groups provide excellent electrode mechanical properties, which effectively alleviate sulfur volume changes during cycling. Furthermore, the -SO_3Li groups also enhance the diffusion of Li^+ in the electrodes. In addition, density functional theory calculations reveal that the Cel-SO_3Li exhibits strong affinity and catalytic ability for LIPSs, indicating that it can effectively suppress the shuttle effect and enhance their reaction kinetics. Therefore, the electrode using Cel-SO_3Li binder reach a high initial discharge capacity of 1165 mAh/g at 0.5 C, remain 545 mAh/g after 1000 cycles with a low capacity decay rate of 0.053 % per cycle. This study proposes the concept of a multifunctional and environmentally friendly binder with the ability of "three birds with one stone" (high adhesion, fast Li^+ diffusion, effective capture and even catalysis for LIPSs), which will contribute to accelerating applications of Li-S batteries.

© 2026 Published by Elsevier B.V. on behalf of Chinese Chemical Society and Institute of Materia Medica, Chinese Academy of Medical Sciences.

Lithium-sulfur batteries (Li-S) have a theoretical specific capacity of 1675 mAh/g and energy density of 2600 Wh/kg, which is considered to be one of the most promising candidate for next generation batteries of portable devices and electric vehicles [1,2]. However, several practical challenges have hindered their commercial application, including shuttle effects caused by lithium polysulfides (LIPSs), significant volume expansion and insulation properties of sulfur and discharge products [3,4].

Many endeavors have already been devoted to addressing these issues, including the development of innovative sulfur host materials [5–8], the creation of multifunctional separators and interlayers [9–11], and the strategic use of electrolyte additives [12,13] to enhance overall battery performance. However, most of strategies introduce an amount of inactive materials, which obviously decrease batteries' energy density. Although binders account for only a modest proportion of the material composition within Li-S batteries' electrodes, their role is crucial in enhancing the cycle life and rate capability of these batteries [14–16]. Polyvinylidene fluoride (PVDF) is commonly employed in Li-S batteries due to its high thermal stability and broad electrochemical stability range [17]. However, PVDF's halogenated components display a notably weak affinity towards LIPSs, which impedes its effectiveness in curtailing notorious shuttle effect and preserving active sulfur content, thereby diminishing the cycling stability of Li-S batteries [18,19]. Yan *et al.* presented a novel PEI-ER binder containing NH_2, -NH-, and -OH. Its nitrogen and oxygen atoms form coordination bonds with lithium atoms, which had strong fixation ability for LIPSs [20]. Liu *et al.* developed a conductive binder of poly(9,9-dioctylfluorene-*co*-fluorenone-*co*-methylben zoic ester) with an integrated carbonyl group. The binder exhibited high binding energy with LIPSs *via* Li-O band, effectively suppressing the shuttle effect in Li-S batteries [21]. Nevertheless, like PVDF, these binders are not water-soluble, which inevitably involves the utilization of toxic organic solvents (such as *N*-methyl-2-pyrrolidone) in the process of electrode preparation, further increases the production cost and pollutes the environment [22]. Ling *et al.* adopted carrageenan, a water-soluble binder that utilizes the nucleophilic substitution

* Corresponding author.
E-mail address: xuebu@cqut.edu.cn (X. Hu).

https://doi.org/10.1016/j.cclet.2025.110985
1001-8417/© 2026 Published by Elsevier B.V. on behalf of Chinese Chemical Society and Institute of Materia Medica, Chinese Academy of Medical Sciences.

reactions between its sulfate groups and LIPSs to effectively thwart the shuttle effect [23]. Although these binders have achieved excellent performance for Li-S batteries, their emphasis is primarily the capture performance of LIPSs while rarely consider the enhancement of Li^+ diffusion ability and the acceleration of redox reaction kinetics [24,25]. Based on the above considerations, a satisfactory binder should have the characteristics of stable mechanical properties, fast Li^+ diffusion, strong capture and even catalytic conversion ability for LIPSs, safety and environmental protection, which significantly enhances the overall performance and application potential of Li-S batteries.

Herein, a novel aqueous lithiated polysaccharide derivative, lithium sulfonated cellulose (Cel-SO_3Li), is designed and prepared for sulfur cathode. Due to special molecular structure, it improves inherent problems of Li-S batteries in various aspects: (1) Anchoring and catalytic conversion of LIPSs: the Cel-SO_3Li with -SO_4Li groups that can capture LIPSs, even contribute to their oxidation–reduction kinetics. (2) Stable mechanical properties: the Cel-SO_3Li is rich in hydroxyl and provides excellent bonding performance, which effectively suppress volume expansion of sulfur. (3) Rapid Li^+ diffusion: the –SO_3Li group in the Cel-SO_3Li can promote the diffusion of Li^+ in Li-S batteries. Consequently, at 0.5 C, the discharge capacity of Li-S batteries using the Cel-SO_3Li binder can maintain at 545 mAh/g after 1000 cycles, with a capacity decay rate of only 0.053 % per cycle. In addition, the Li-S batteries using Cel-SO_3Li binder can provide 754 mAh/g capacity at 2 C, demonstrating well rate performance.

The binder is highly important as a necessary component to stabilize the electrodes in batteries. As shown in Fig. 1a, large volume expansion, active material exfoliation, LIPSs dissolution and slow reaction kinetics will happen in electrodes using PVDF binder during cycling. Compared to PVDF, multifunctional Cel-SO_3Li binder with rich hydroxyl can provide excellent mechanical properties and inhibit the electrode volume expansion. In addition, Li^+ in the binder effectively enhances Li^+ diffusion rate of the electrodes (Fig. 1b). More importantly, as shown in Fig. 1c, functional groups -SO_4 can react with LIPSs in nucleophilic substitution reaction, which effectively captures LIPSs and accelerates the kinetics of LIPSs conversion reaction. The Cel-SO_3Li binder with rich -SO_3Li groups is synthesized by esterification of refined cotton (RC) with sulfur trioxide pyridine complex (Fig. S1 in Supporting information). To verify the structural difference between RC and Cel-SO_3Li, Fourier transform infrared spectroscopy (FTIR) is conducted (Fig. 1d). The peaks at 814 and 1225 cm^{-1} are the stretching vibration peak of C-O-S and the asymmetric stretching vibration peak of O=S=O, proving the presence of -SO_4 group characteristic peak. The fact indicates that the H of the hydroxyl group on the cellulose structural unit is replaced by -SO_3 group, meaning the sulfonation reaction occurs. The results of element content for RC and Cel-SO_3Li are shown in Fig. 1e. Clearly, the contents of Li, C and S in Cel-SO_3Li are 4.73 %, 18.72 % and 21.56 %, indicating the successful introduction of -SO_3Li group. The total degree of substitution (DS) of -SO_3Li group is calculated by the following formula:

$$DS = (72.066 \times S\%)/(32.06 \times C\%) \quad (1)$$

According to the calculation of equation, the DS reaches 2.59, which indicates that average 2.59 hydroxyl groups have undergone substitution reactions on each cellulose unit. The above results show that the -SO_3Li group is successfully substituted on cellulose and have a high DS.

As a strong nucleophilic reagent, LIPSs can attack the activated carbon (C) site attached to the leaving group, resulting in the formation of a new C-S bond [26]. Fig. 2a shows the process of nucleophilic substitution reaction. The -SO_4Li in Cel-SO_3Li acts as a leaving group to form a new C-S bond with LIPSs. The mecha-

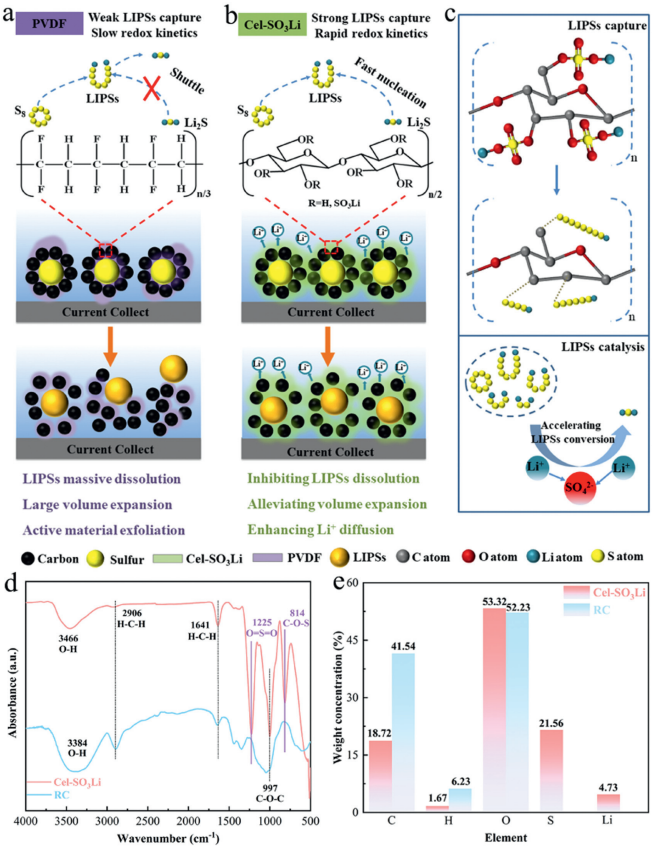


Fig. 1. (a) The sulfur electrode with PVDF binder has the characteristics of slow redox kinetics, large volume expansion and LIPSs dissolution. (b) Schematic diagram of Cel-SO_3Li binder sulfur electrode, with fast redox kinetics and small volume expansion, and anchoring LIPSs in the electrochemical process. (c) Schematic diagram of the mechanism of immobilization and catalysis of LIPSs by Cel-SO_3Li binder. (d) FTIR spectra of RC and Cel-SO_3Li. (e) Elemental content of RC and Cel-SO_3Li.

nism is further explained by visible adsorption experiments and Ultraviolet-visible (UV–vis) spectroscopy. Fig. S2 (Supporting information) depicts the visible color alterations after the addition of Cel-SO_3Li and PVDF respectively. After 24 h, the dark yellow of the Li_2S_6 solution containing Cel-SO_3Li become clear but the solution containing PVDF keeps almost unchanged. The results indicate that plenty of -SO_4Li group is replaced by LIPSs, proving more LIPSs are captured. UV–vis spectra further verify the capture capacity of Cel-SO_3Li binder to LIPSs and the results are shown in Figs. 2b and c. Clearly, the peak at 430 nm means the characteristic absorption of Li_2S_6 [27]. With the passage of time, the characteristic peak intensity rapidly decreases in Li_2S_6 solution containing Cel-SO_3Li. However, the peak intensity remains stable in the solution containing PVDF. Above facts shows that Cel-SO_3Li binder have a strong ability to capture LIPSs, which is due to the formation of grafted LIPSs originated from the substitution reaction between -SO_4Li and dissolved LIPSs. In order to reveal the reaction rate between different binders and LIPSs, the reaction kinetics diagram based on UV–vis is shown in Fig. S3 (Supporting information). Clearly, PVDF has small physical absorption in the initial stage and reach equilibrium after about 300 min. On the contrast, the substitution reaction between Cel-SO_3Li and LIPSs happen slowly but continuously. Fig. 2d shows the FTIR spectra of Cel-SO_3Li before and after absorption in LIPSs solution. Clearly, a new characteristic peak appeared at 1100 cm^{-1} after absorption, which is due to the C-S bond. The results indicate the occurrence of nucleophilic substitution reaction between Cel-SO_3Li and LIPSs. The XPS of Cel-SO_3Li before and after the absorption in Li_2S_6 solution further prove the occurrence of the sub-

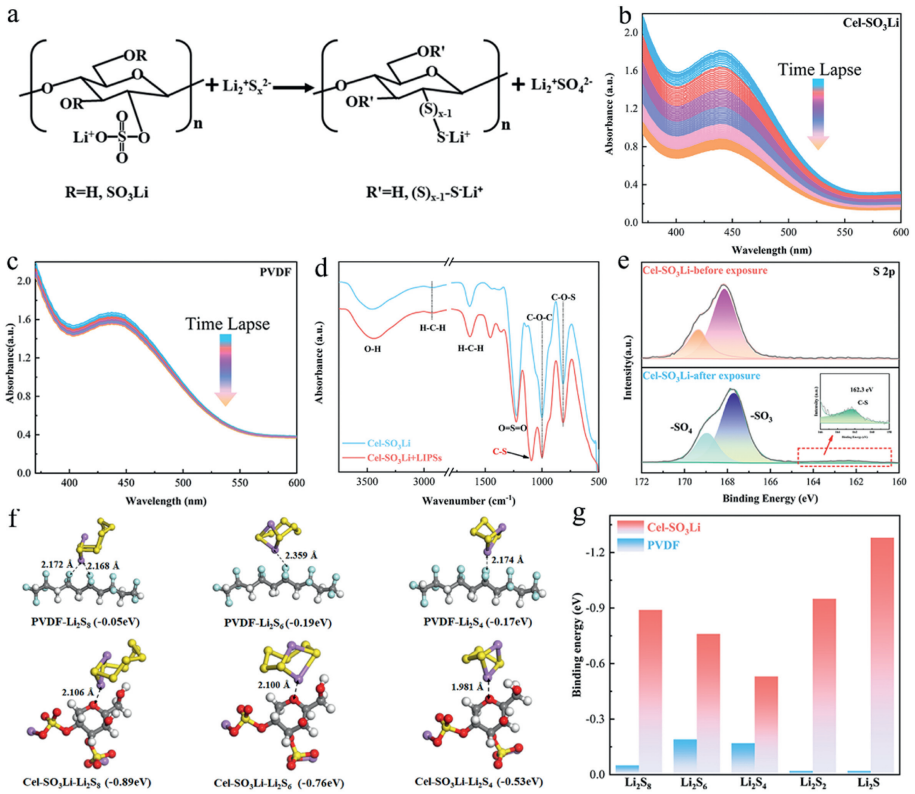


Fig. 2. (a) Molecular structures of Cel-SO_3Li and their replacement reactions with LIPSs to form immobilized LIPSs on the polymer backbones. (b, c) UV–vis spectral profiles for Cel-SO_3Li and PVDF in Li_2S_6 solutions. (d) FTIR analysis for Cel-SO_3Li pre and post interaction with LIPSs solutions. (e) XPS analysis for Cel-SO_3Li pre and post interaction with LIPSs solutions. (f, g) Bond lengths and binding energies between Cel-SO_3Li, PVDF, and long-chain LIPSs.

stitution reaction (Fig. 2e). As expected, a new peak appears at 162.3 eV after the absorption, which is attributed to the formation of the C-S bond and also confirms the substitution reaction between Cel-SO_3Li and LIPSs. Moreover, the characteristic peaks of -SO_3 and -SO_4 in Cel-SO_3Li are located at 168.1 and 169.4 eV, respectively. After LIPSs adsorption, they shift towards lower binding energies 167.7 and 169.0 eV, indicating a strong chemical interaction between Cel-SO_3Li and LIPSs [28,29]. Notably, the formation of the C-S bond is beneficial for mitigating LIPSs dissolution and suppressing shuttling effects, and thus improving the cycle stability of sulfur electrodes. The discharge test of the visual Li-S batteries is employed to further verify the strong capture capacity of Cel-SO_3Li binder on LIPSs during the discharge process. The results are shown in Fig. S4 (Supporting information). Meanwhile, the photos of Cel-SO_3Li and PVDF based batteries separators after cycling also demonstrate the inhibitory effect of Cel-SO_3Li on LIPSs (Fig. S5 in Supporting information). To reveal effective interaction between Cel-SO_3Li and LIPSs, the binding energy and bond length between the two binders and LIPSs are calculated [30–32]. As shown in Figs. 2f and g and Fig. S6 (Supporting information), the binding energies of Cel-SO_3Li-Li_2S_8 (−0.89 eV), Cel-SO_3Li-Li_2S_6 (−0.76 eV) and Cel-SO_3Li-Li_2S_4 (−0.53 eV) are higher than PVDF-Li_2S_8 (−0.05 eV), PVDF-Li_2S_6 (−0.19 eV) and PVDF-Li_2S_4 (−0.17 eV), and the bond length between LIPSs and Cel-SO_3Li is smaller than that of PVDF. These results indicate that Cel-SO_3Li exhibits significant affinity for LIPSs, effectively mitigating the shuttle effect and significantly enhancing the electrochemical performance of Li-S batteries.

In order to confirm the superiority of Cel-SO_3Li binder for Li-S batteries, different binders (Cel-SO_3Li and PVDF) are used to monitor the symmetrical batteries. As depict in Fig. 3a, Li_2S_6 symmetrical batteries incorporating the binder delivers a stronger current response compared to that of PVDF binder at 0.2 mV/s, proving improved conversion ability between LIPSs and Li_2S. The Cel-SO_3Li binder without Li_2S_6 shows no oxidation and reduction peaks, suggesting that the binder is electrochemically stable during the cycle, and the change of the peaks is attributed to the interaction between Cel-SO_3Li and LIPSs [33]. Furthermore, the nucleation behavior of Li_2S is examined through current-time transient spectroscopy to substantiate the improved conversion capability of LIPSs using the Cel-SO_3Li binder [34]. As shown in Figs. 3b and c, as the rate limiting step for slow sulfur redox reactions, the response time and current strength for the electrode position of Li_2S nucleation in the Cel-SO_3Li electrode are earlier and stronger than those in the PVDF electrode. Correspondingly, the Li_2S deposition capacity of 118.8 mAh/g in the Cel-SO_3Li electrode is higher than 64.7 mAh/g of PVDF electrode, indicating that the Cel-SO_3Li could effectively promote liquid-solid phase conversion. The nucleation and growth rate of Li_2S can be determined by the nucleation and growth rate constant (Ak^2). The nucleation and growth rate constant can be obtained using equations [35].

$$Ak^2 = 2/\pi t_m^3 \quad (2)$$

where A means the nucleation rate constant (cm^{-2} s^{-1}), k represents the growth rate (cm/s). As shown in Fig. S7 (Supporting information), the growth rate of Li_2S nucleation using the Cel-SO_3Li is higher than that using the PVDF, suggesting that the Cel-SO_3Li binder achieves rapid kinetics of Li_2S deposition. To further verify catalytic performance of Cel-SO_3Li, CV measurements are carried out on the batteries with different binders. Fig. 3d reveals that the Cel-SO_3Li electrode shows higher peak intensities and lower redox potentials, indicating that its kinetic performance is improved and the degree of electrochemical polarization is reduced. Moreover, Ic_1, Ic_2 and Ia_1 of Tafel slopes in Cel-SO_3Li electrode are 51.9, 49.5 and 44.3 mV/dec, respectively, which is lower than 81.9, 89.3 and 63.4 mV/dec in the PVDF (Figs. 3e and f, Fig. S8 in Supporting information) [36]. The fact further confirmed that the Cel-SO_3Li

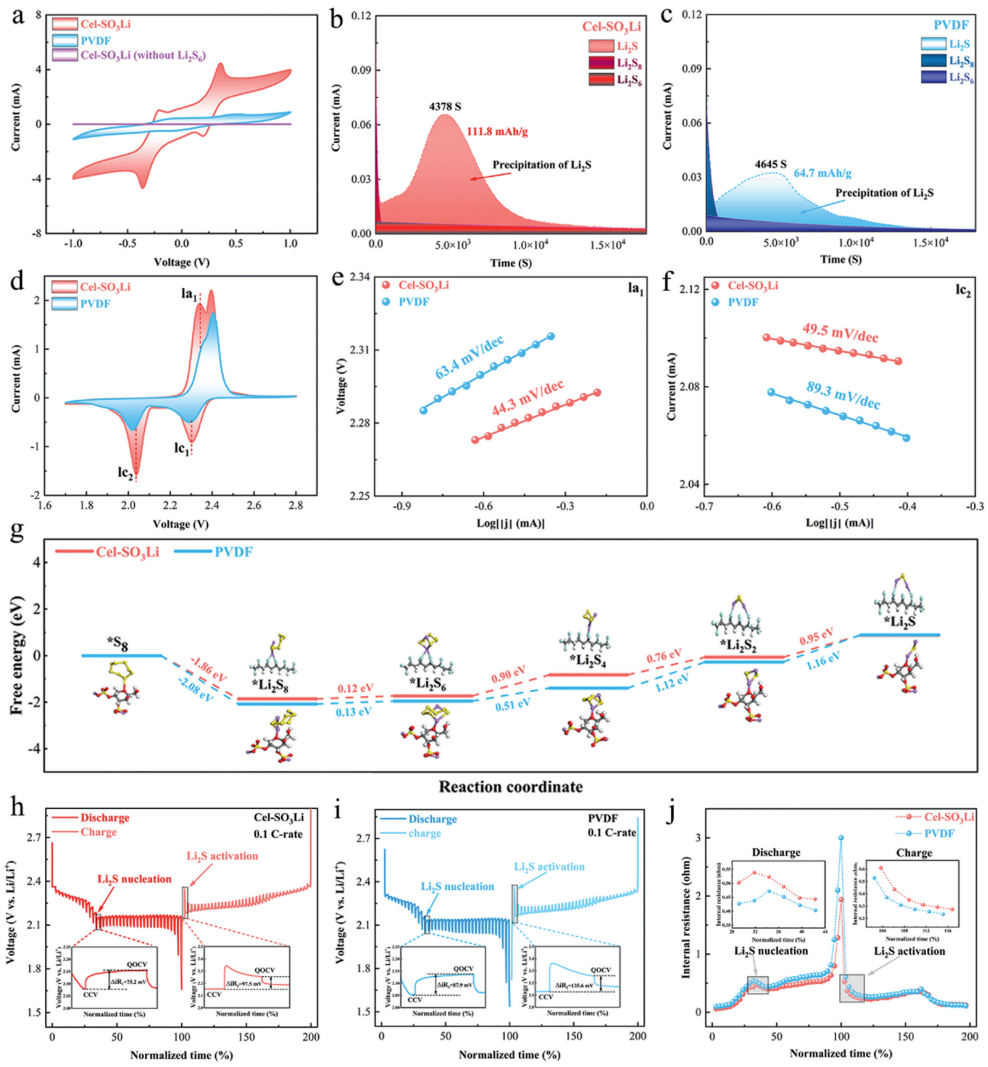


Fig. 3. (a) Electrochemical characterization *via* CV for symmetrical batteries using various binders. (b, c) Current responses during the potentiostatic deposition of Li_2S across electrodes with different binders. (d) Electrochemical curves *via* CV for batteries incorporating diverse binders. Tafel analyses for (e) anodic peak Ia_1 and (f) cathodic peak Ic_2 from part (a). (g) Energy profiles of Gibbs free energy for Cel-SO_3Li and PVDF when interacting with LIPSs (Li_2S_n, where $1 \leq n \leq 8$), along with their corresponding optimized structural models. (h, i) Display galvanostatic intermittent titration technique (GITT) analyses for Cel-SO_3Li and PVDF electrodes. (j) Internal resistances of Cel-SO_3Li and PVDF electrodes with respect to normalized charge/discharge time.

has a positive effect on the dynamics of LIPSs. The transformation of sulfur species is theoretically analyzed to calculate the Gibbs free energy *via* density functional theory [37]. Fig. 3g illustrates the conversion process from Li_2S_8 to Li_2S. Obviously, the Gibbs free energies of the Cel-SO_3Li are significantly lower than those of PVDF, indicating that Cel-SO_3Li could effectively accelerate the catalytic conversion of LIPSs. The rate limiting step from Li_2S_2 to Li_2S has highest Gibbs free energy. The value in the Cel-SO_3Li is 0.95 eV, which is lower than 1.16 eV of PVDF, indicating that the Li_2S nucleation efficiency in the Cel-SO_3Li is higher. These results are consistent with the conclusions of Figs. 3b and c.

The reaction and diffusion kinetics for PVDF and Cel-SO_3Li electrodes are investigated by constant current intermittent titration (GITT). As shown in Figs. 3h and i, the Cel-SO_3Li electrode have smaller voltage change (ΔiR, 75.2 and 97.5 mV) between *quasi*-open-circuit-voltage (QOCV) and closed-circuit-voltage (CCV) compare to 87.9 and 135.6 mV of PVDF electrode, indicating that it have faster redox kinetics. In addition, the Cel-SO_3Li electrode shows low internal resistance ($\Delta R_{internal}$), especially in nucleation and activation process of Li_2S, which indicate that the Cel-SO_3Li binder improved Li^+ diffusion rate and accelerate Li_2S nucleation and activation in Li-S batteries (Fig. 3j) [38]. The CV curves of different electrodes at different scanning rates are shown in Figs. S9a and b (Supporting information). Clearly, the Cel-SO_3Li electrode has good electrochemical stability compared to the PVDF electrode. As suggested by the Randles-Sevcik equation, Li^+ diffusion coefficient is evaluated from the slope of the curve fitted from the peak current versus the square root of the scanning rate in CV profiles [39,40]. The slope of the Cel-SO_3Li electrode is larger than that of PVDF (Figs. S9c and d in Supporting information), demonstrating better Li^+ diffusion. EIS and Warburg impedance coefficient (σ) further confirm the rapid diffusion of Li^+ in the Cel-SO_3Li electrode (Figs. S10a-d, Tables S1 and S2 in Supporting information) [41]. Fig. S11 (Supporting information) displays the excellent adhesion performance of the Cel-SO_3Li binder. Figs. S12a-d (Supporting information) show surface morphology of the electrodes using different binders, indicating that Cel-SO_3Li electrode has excellent mechanical properties. Figs. S12e-h (Supporting information) display cross-sectional views of electrodes using various binders before and after cycling, demonstrating that the Cel-SO_3Li binder significantly mitigate the electrode volume expansion. Fig. S13 (Supporting information) depicts that the degree of swelling observed in

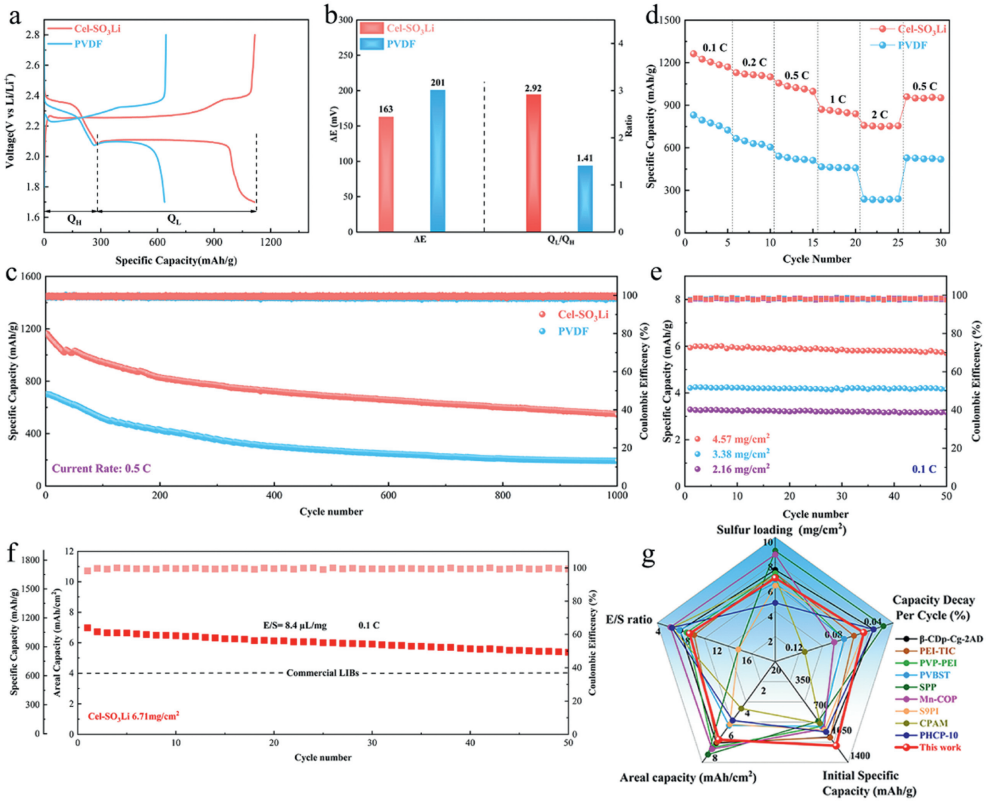


Fig. 4. (a) Electrochemical profiles for sulfur cathodes incorporating various binders at 0.2 C. (b) Measurements of ΔE and C_{LO}/C_{UP} derived from the electrochemical profiles at 0.2 C. (c) Cycling performance and Coulombic efficiency of sulfur cathodes with different binders at 0.5 C. (d) Discharge rate capacities of sulfur cathodes utilizing different binders. (e) Cycling performance of Cel-SO_3Li electrode with different S-loaded and a relatively low E/S ratio. (f) Cycling performance of Cel-SO_3Li electrode with 6.71 mg/cm^2 S-loaded (E/S = 8.4). (g) Compare the integrated electrochemistry performance with other current reported binders, such as β-CDp-Cg-2AD [48], PEI-TIC [49], PVP-PEI [32], PVBST [50], SPP [51], Mn-COP [52], S9PI [53], CPAM [54], PHCP-10 [55].

PVDF is considerably greater than that in Cel-SO_3Li [42]. Figs. S14 and S15 (Supporting information) demonstrate the surface uniformity of different electrodes. Compared to the Cel-SO_3Li electrode, the surface aggregation of the PVDF electrode is more serious and its surface is much rougher. As shown in Figs. S16a-f (Supporting information), the binding energy between Cel-SO_3Li binder and active/conductive/collector materials is greater than PVDF, indicating that the adhesion between Cel-SO_3Li binder and active, conductive and current collector materials in sulfur electrode is much stronger than PVDF binder. The conclusions are consistent with the results of Figs. S16g and h (Supporting information).

Fig. 4a compares the charge/discharge profiles for the electrodes at 0.2 C. As shown in Fig. 4a, the Cel-SO_3Li electrode demonstrates a notably greater discharge capacity than the PVDF electrode. The noted potential difference (ΔE) between the oxidation and reduction stages at a 50 % discharge capacity highlights the extent of polarization during the redox reactions [43]. Clearly, the ΔE of 163 mV in the Cel-SO_3Li electrode is lower than 201 mV in the PVDF (Fig. 4b). For the discharging process, the curve can be divided into two parts: Q_{UP} from the dissolution stage and Q_{LO} from the deposition stage. In theory, the Q_{LO}/Q_{UP} value of Li-S batteries is 3. The closer to 3 the Q_{LO}/Q_{UP} value, the better the conversion reaction of the LIPSs [44]. The Cel-SO_3Li electrode reach a Q_{LO}/Q_{UP} ratio of 2.92 compared to 1.41 of the PVDF electrode, indicating that the Cel-SO_3Li binder effectively improve the liquid-solid conversion rate. Above results prove that the Cel-SO_3Li binder can immobilize LIPSs, thereby promoting the oxidation–reduction reaction kinetics of LIPSs and improving the electrochemical performance of Li-S batteries. Fig. 4c evaluates long-term cycling stability of the electrodes at 0.5 C. Clearly, the Cel-SO_3Li electrode have an initial discharge capacity of 1165 mAh/g and stabilize at 545 mAh/g even after 1000 cycles, with a decay rate per cycle of 0.053 %. In contrast, the corresponding values in the PVDF electrode are 701 mAh/g, 205 mAh/g and 0.071 %. Fig. S17 (Supporting information) shows the cycling performance of the cathodes with different contents of Cel-SO_3Li. Clearly, the cathode with 5 wt% Cel-SO_3Li possesses best cycling stability. Figs. S18a and b (Supporting information) show the charge/discharge profiles of the electrodes at different cycle numbers. Clearly, the ΔE of the corresponding cycles in the Cel-SO_3Li electrode (from 197 mV to 268 mV) is all lower than those in the Cel-SO_3Li (from 247 mV to 308 mV) (Fig. S18c in Supporting information). These findings are coincided with the conclusion in Fig. 4b. As shown in Figs. S18d and e (Supporting information) both high and low plateaus of the Cel-SO_3Li electrode are stable and provided high discharge capacities compared to wide voltage fluctuation of PVDF electrode, indicating that the Cel-SO_3Li effectively suppress the production of LIPSs [45]. After the 100th discharge, S utilization rate of the Cel-SO_3Li electrode in Q_{UP} and Q_{LO} process reach 19.42 % and 36.75 % (total 56.17 %), which is much higher than 10.52 % and 20.71 % (total 31.23 %) in the PVDF electrode (Fig. S18f in Supporting information). The results indicate that the Cel-SO_3Li electrode has higher sulfur utilization and LIPSs conversion than the PVDF electrode.

Displayed in Fig. 4d are the comparative rate performances of two distinct electrodes. The electrode incorporating the Cel-SO_3Li binder consistently outperforms the PVDF counterpart in terms of discharge capacity at various rates. Specifically, the electrode using Cel-SO_3Li binder reaches a capacity of 754 mAh/g at 2.0 C. When back to 0.5 C, its capacity increases to 950 mAh/g and the recovery rate is 97.4 % compare to 529 mAh/g and 94.9 % of the PVDF elec-

trode, which show that the Cel-SO_3Li electrode have remarkable electrochemical reversibility. Figs. S18g-i (Supporting information) depict the charge/discharge plateaus for two electrodes at different rates. In contrast to the PVDF electrode, the Cel-SO_3Li electrode has a lower degree of polarization. The self-discharge experiments further prove the influence of the Cel-SO_3Li binder on the shuttle effect of LIPSs. As shown in Figs. S19 and S20 (Supporting information), the capacity loss and voltage drop in the Cel-SO_3Li electrode are significantly smaller than those in the PVDF electrode after different resting and recovery times, which indicate that the Cel-SO_3Li binder have well anchoring ability on LIPSs [46]. In-depth investigations are conducted to explore the practicality of utilizing Cel-SO_3Li binder within Li-S batteries, focusing on electrodes characterized by high sulfur content and low electrolyte volume. When the sulfur loading of Cel-SO_3Li electrodes are 2.16, 3.38 and 4.57 mg/cm^2, initial capacity of the battery is 3.29, 4.21 and 5.93 mAh/cm^2, respectively, which could be maintained at 3.14, 4.12 and 5.75 mAh/cm^2 after 50 cycles at 0.1 C (Fig. 4e). Notably, at a sulfur loading of 6.71 mg/cm^2 and a comparatively low E/S ratio of 8.4 μL/mg, the area capacity of the Cel-SO_3Li electrode can reach 6.98 mAh/cm^2 and remain stable capacity of 5.40 mAh/cm^2 after 50 cycles (Fig. 4f), which has exceeded 4 mAh/cm^2 of commercial Li-ion batteries [47]. Comparative analysis of electrochemical performances, depicted in Fig. 4g [32,48–55], underscores the superior balance attained by Cel-SO_3Li binders in terms of cycle life, E/S ratios, sulfur loading, and capacity retention compared to other polymer binders, thereby highlighting their competitive edge in the realm of Li-S batteries.

In summary, a novel water-soluble Cel-SO_3Li binder is proposed to improve overall electrochemical performance of Li-S batteries. The physical and electrochemical experiments prove the Cel-SO_3Li binder possesses multifunctions: (1) Due to the nucleophilic substitution reaction between -SO_4Li and dissolved LIPS, it effectively immobilizes LIPSs and helps accelerate its redox kinetics. (2) It provides excellent mechanical performance and keeps the electrode integrity before and after cycling due to the robust adhesion. (3) It shows high Li^+ diffusion performance due to the -SO_4Li groups. Calculations using density functional theory have corroborated the stabilizing and catalytic roles of Cel-SO_3Li on LIPSs. Based on above advantages, the Cel-SO_3Li electrode exhibits an initial discharge capacity of 1165 mAh/g at 0.5 C, the capacity decay rate per cycle is only 0.053 % after 1000 cycles. Even under high sulfur loading of 6.71 mg/cm^2, the electrode still has a high initial capacity of 6.98 mAh/cm^2. This work provides a cost-effective strategy for practical application of water-soluble binder in high performance Li-S batteries.

Declaration of competing interest

The authors declare that we have no known competing financial interests or personal relationships that could have appeared to influence the work reported in this paper.

CRediT authorship contribution statement

Wenyang Lei: Writing – original draft, Investigation, Formal analysis, Data curation. **Zhenwei Li:** Methodology. **Hao He:** Conceptualization. **Lan Yang:** Validation. **Xuebu Hu:** Writing – review & editing, Supervision, Resources, Project administration, Funding acquisition. **Wei Liao:** Writing – review & editing. **Xiaowen Yu:** Supervision. **Zhongli Hu:** Project administration.

Acknowledgments

This work was supported by Chongqing Natural Science Foundation (Nos. CSTB2023NSCQ-LZX0039, CSTB2023NSCQMSX0405), the Key Project of Chongqing Technology Innovation and Application Development (No. CSTB2023TIAD-KPX0091) and the National Natural Science Foundation of China (No. 22309022).

Supplementary materials

Supplementary material associated with this article can be found, in the online version, at doi:10.1016/j.cclet.2025.110985.

References

[1] M. Li, J. Lu, Z. Chen, K. Amine, Adv. Mater. 30 (2018) 1800561.
[2] R. Schmuch, R. Wagner, G. Hörpel, T. Placke, M. Winter, Nat. Energy 3 (2018) 267–278.
[3] H. Ding, Z.H. Chen, H.Y. Li, et al., Nano Lett. 24 (2024) 15118–15126.
[4] R.N. Guo, Y. Yang, X.L. Huang, et al., Adv. Funct. Mater. 34 (2023) 2307108.
[5] Y. Wang, X. Chen, F. Yu, et al., Chin. Chem. Lett. 35 (2023) 109001.
[6] C.C. Zhao, F. Huo, Y. Yang, et al., Adv. Funct. Mater. 34 (2024) 2402175.
[7] F.X. Liang, Y.Z. Zhu, N.N. Wang, et al., Chin. Chem. Lett. 35 (2024) 109461.
[8] S. Yu, Y.G. Zhang, S. Yang, et al., Chin. Chem. Lett. 34 (2023) 107911.
[9] W. Zhang, X. Du, M. Zhang, et al., J. Colloid Interf. Sci. 663 (2024) 735–748.
[10] H. Wang, X. Lai, C. Chen, et al., Chin. Chem. Lett. 35 (2023) 108473.
[11] X. Wu, N. Liu, Z. Guo, et al., Energy Storage Mater. 28 (2020) 153–159.
[12] J. Sun, K. Zhang, Y. Fu, W. Guo, Nano Res. 16 (2022) 3814–3822.
[13] Y. Liu, Y. Elias, J. Meng, et al., Joule 5 (2021) 2323–2364.
[14] S. Ma, G.Y. Wan, Z.Y. Yan, X.C. Liu, T.Z. Chen, Chin. Chem. Lett. 36 (2025) 109853.
[15] X.X. Gu, Z.G. Yang, S. Qiao, et al., Rare Metals 40 (2021) 529–536.
[16] J. Zhang, M. Li, H.A. Younus, et al., Nano Mater. Sci. 3 (2021) 124–139.
[17] Y. Wu, Y. Li, Y. Wang, et al., J. Energy Chem. 64 (2022) 62–84.
[18] X. Liu, T. Qian, J. Liu, et al., Small 14 (2018) 1801536.
[19] J. Liu, D.G.D. Galpaya, L. Yan, et al., Energy Environ. Sci. 10 (2017) 750–755.
[20] L. Yan, X. Gao, F. Wahid-Pedro, et al., J. Mater. Chem. A 6 (2018) 14315–14323.
[21] G. Ai, Y. Dai, Y. Ye, et al., Nano Energy 16 (2015) 28–37.
[22] L. Ibing, T. Gallasch, P. Schneider, et al., J. Power Sources 423 (2018) 183–191.
[23] M. Ling, L. Zhang, T. Zheng, et al., Nano Energy 38 (2017) 82–90.
[24] Y. Huang, M. Shaibani, T.D. Gamot, et al., Nat. Commun. 12 (2017) 5375.
[25] P.D. Frischmann, Y. Hwa, E.J. Cairns, B.A. Helms, Chem. Mater. 28 (2016) 7414–7421.
[26] H.F. Shi, W.Y. Sun, J.K. Cao, et al., Adv. Funct. Mater. 33 (2023) 2306933.
[27] W.S. Heo, W. Kwon, T. Lee, et al., Small Methods 8 (2024) 2301401.
[28] J. Xu, L. Xu, Z. Zhang, et al., Energy Storage Mater. 47 (2022) 223–234.
[29] S. Chen, J. Zhang, Z. Wang, et al., Nano Lett. 21 (2021) 5285–5292.
[30] C. He, C. Xu, W.X. Zhang, ACS Appl. Mater. Interfaces 15 (2023) 57015–57028.
[31] W. Jiang, T. Zhang, R. Mao, et al., eScience 4 (2024) 100203.
[32] R. Gao, Q. Zhang, Y. Zhao, et al., Adv. Funct. Mater. 32 (2022) 2110313.
[33] Y. Li, W. Wang, X. Liu, et al., Energy Storage Mater. 23 (2019) 261–268.
[34] A. Gupta, A. Manthiram, J. Mater. Chem. A. 9 (2021) 13242–13251.
[35] M.X. Wang, L.S. Fan, X. Sun, et al., ACS Energy Lett. 5 (2020) 3041–3050.
[36] C. Li, W. Ge, S. Qi, et al., Adv. Energy Mater. 12 (2022) 2103915.
[37] Y.B. Wu, C. He, W.X. Zhang, J. Am. Chem. Soc. 144 (2022) 9344–9353.
[38] S. Guo, Y. Xiao, J. Wang, Y, et al., Nano Res. 14 (2021) 4556–4562.
[39] Z. Liang, D. Yang, P. Tang, et al., Adv. Energy Mater. 11 (2020) 2003507.
[40] M. Wang, L. Fan, Y. Qiu, et al., J. Mater. Chem. A. 6 (2018) 11694–11699.
[41] H. Zhang, L. Yang, P. Zhang, et al., Adv. Mater. 33 (2021) 2008447.
[42] D. Yao, J. Feng, J. Wang, Y. Deng, C. Wang, J. Power Sources 463 (2020) 0378–7753.
[43] C. Zhang, J.J. Biendicho, T. Zhang, et al., Adv. Funct. Mater. 29 (2019) 1903842.
[44] D. Su, M. Cortie, H. Fan, G. Wang, Adv. Mater. 29 (2017) 1700587.
[45] C. Senthil, S.S. Kim, H.Y. Jung, Nat. Commun. 13 (2022) 145.
[46] Z.Z. Chen, M.J. Lu, Y. Qang, et al., Adv. Energy Mater. 13 (2023) 2300092.
[47] H.J. Peng, J.Q. Huang, Q. Zhang, Chem. Soc. Rev. 46 (2017) 5237–5288.
[48] T. Zhang, R. Mao, W. Jiang, et al., Nano Energy 114 (2023) 108603.
[49] T. Zhang, B. Li, Z. Song, et al., Energy Environ. Mater. 7 (2023) 12572.
[50] M. Si, X. Jian, Y. Xie, et al., Adv. Energy Mater. 14 (2024) 2303991.
[51] H. Wang, Y. Yang, P. Zheng, et al., Chem. Eng. J. 395 (2020) 124981.
[52] X. Yao, C. Guo, C. Song, M. Lu, et al., Adv. Mater. 35 (2023) 2208846.
[53] H. Wang, Y. Wang, G. Zhang, et al., Electrochim. Acta 371 (2021) 137822.
[54] S. Li, W. Xiao, H. Do, et al., Small 18 (2022) 2107109.
[55] M. Liu, P. Chen, X. Pan, et al., Adv. Funct. Mater. 32 (2022) 2205031.